Molecular Modeling for Calculation of Mechanical Properties of

Epoxies with Moisture Ingress

T.C. Clancy[*], S.J.V. Frankland[*]
National Institute of Aerospace
100 Exploration Way
Hampton, VA 23666

J.A. Hinkley[†], T.S. Gates[‡]
NASA Langley Research Center
Hampton, VA 23681

Abstract
Atomistic models of epoxy structures were built in order to assess the effect of crosslink degree, moisture content and temperature on the calculated properties of a typical representative generic epoxy. Each atomistic model had approximately 7000 atoms and was contained within a periodic boundary condition cell with edge lengths of about 4 nm. Four atomistic models were built with a range of crosslink degree and moisture content. Each of these structures was simulated at three temperatures: 300 K, 350 K, and 400 K. Elastic constants were calculated for these structures by monitoring the stress tensor as a function of applied strain deformations to the periodic boundary conditions. The mechanical properties showed reasonably consistent behavior with respect to these parameters. The moduli decreased with decreasing crosslink degree with increasing temperature. The moduli generally decreased with increasing moisture content, although this effect was not as consistent as that seen for temperature and crosslink degree.

1. Introduction

Epoxies are useful compounds in many applications. In aerospace applications, they are used as adhesives as well as matrix components in composites. The effects of hygrothermal aging on epoxy materials are difficult to predict. Hygrothermal aging typically refers to the deterioration of the performance of a material due to prolonged exposure to moisture and variable temperature conditions. In this paper, structural

---

[*] Resident at Durability, Damage Tolerance and Reliability Branch, NASA-LaRC
[†] Advanced Materials and Processing Branch
[‡] Durability, Damage Tolerance and Reliability Branch

features associated with hygrothermal aging are studied with atomistic level computer simulation. The assumption is made that variables such as crosslinking degree and moisture content will vary with time and exposure to environmental conditions.

Water absorption in epoxies can be a complex process even under controlled laboratory conditions. Experimental studies have found water to exist in both "free" and "bound" states[1]. Additional studies have even found two different "bound" states for water in epoxy[2]. Absorption of water can bring about both reversible and irreversible changes to the epoxy resin[3]. However, it is reasonable to assume that water content will generally increase with exposure to humid or wet environments and reach a saturation value. Under certain conditions, the modulus of the resin can increase with absorbed water due to strong dipole-dipole interactions[2, 4]. Generally, however, water plasticizes the epoxy, reducing properties such as modulus and glass transition temperature, T_g [5, 6]. Chemical bonds can break due to hydrolysis and thermo-oxidative aging, effectively reducing the crosslinking degree in the cured epoxy[7]. Crosslinking reactions can also continue in an epoxy over time resulting in increased stiffness[8].

Given these complex relationships between the aging process and these two structural features of interest (moisture content and degree of crosslinking), the effect of hygrothermal aging is not directly studied. Rather, in this initial work, quantitative values for mechanical properties are predicted as a function of these structural features and temperature in the atomistic models. Although time dependence is not considered directly here, these molecular structural features known to vary with time and exposure are considered. Therefore, aging effects on these epoxy models are studied indirectly.

Fully atomistic simulations of macromolecular systems can be difficult to construct because of the range of length scales involved and the complexity of the bonding. Most fully atomistic simulations of polymers involve amorphous linear polymers and the chain lengths are typically oligomeric in scale. Crosslinked polymers, such as epoxies, have highly connected complex molecular architectures. Due to the complex structure of crosslinked polymers, only a limited amount of research has been conducted in the fully atomistic modeling of crosslinked macromolecular structures. A method was developed recently for building crosslinked atomistic structures[9]. This method involves the instantaneous bond formation of crosslinks between reactant species. This basic method has been used with some modification for most atomistic simulations of crosslinked macromolecules[10-12].

The atomistic modeling of polymers for calculating mechanical properties has been researched for several decades. A static method was developed early on using molecular mechanics (MM) techniques[13]. Stress-strain simulations in molecular dynamics (MD) have been employed for some time[14]. However, performing these simulations is not a trivial task. It can be difficult to obtain mechanical properties from atomistic simulation that compare well with experimentally measured values due to the difficulty of preparing the models and the various parameters involved[15, 16]. A comparably high rate of strain is necessary in these simulations due to the short time scales of MD simulations as compared to experimentally accessible time scales. Atomistic MD simulations typically employ the integration of time steps 1 fs in duration. A feasible (computationally affordable) run might employ 10^5 to perhaps 10^6 time steps, which would be a duration of 10^2-10^3 ps.

The organization of this paper is as follows. In section 2 of this paper, the methodology for building these atomistic models and calculating the properties is described. In section 3, results obtained from these simulations are presented. In section 4, the conclusions are presented.

2. Methodology

In this section, the methods used for generating the models and calculating the properties of these models are described. The details of the molecular species and the force field are listed. In section 2.1, the methodology for constructing the crosslinked network is described. In section 2.2, the method for calculating the elastic constants is presented.

2.1. Modeling of epoxies and crosslinked polymers

Fig. 1 shows the reactant molecules. The molecule containing the epoxy groups is the diglycidyl ether of bisphenol A (DGEBA) shown in Fig. 1a. There are two isomers for the reactant containing the crosslinking amine groups, diethyltoluene diamine (DETDA) shown in Figs. 1b-c. These two isomers are nearly identical. The second amine group is bonded to the number 4 toluene ring carbon atom in the isomer in Fig. 1b, while the second amine is bonded to the number 6 toluene carbon atom in the isomer in Fig. 1c. There were 108 DGEBA molecules and 54 DETDA molecules in this simulated mixture for a total of 6966 atoms. There were 42 molecules of the isomer shown in Fig. 1b and 12 molecules of the isomer shown in Fig. 1c. This ratio comes from the known ratio of these isomers in commercially available samples of DETDA[17]. Fig. 2 shows the chemical reaction which takes place between the epoxide functional groups in the DGEBA reactant and the amine functional groups in the DETDA reactant. In Fig. 2a, a

primary amine group reacts with an epoxide group to form a chemical bond between the nitrogen of the amine and the terminal carbon of the epoxide group. The carbon-oxygen bond breaks between the terminal carbon and the epoxide oxygen, leaving an alcohol functional group. In Fig. 2b, the product of the reaction depicted in Fig. 2a undergoes further reaction with an additional epoxide group. The nitrogen atom now forms the center of a crosslinked molecular architectural structure.

The AMBER force field[18, 19] was used in simulating these structures. The TIP3P[20] parameters were used to simulate the water in these simulations. Charges were estimated by using a bond decrement method used for the CVFF force field in the Materials Studio software[21]. This bond decrement method assigns equal magnitude, opposite sign charges to each pair of atoms connected by a bond. This produces a consistent, if approximate charge assignment. The LAMMPS[22] software was used to run these molecular mechanics (MM) and molecular dynamics (MD) simulations. Molecular mechanics typically refers to energy minimization techniques applied to static structures. Molecular dynamics involves the integration of the classical equations of motion of a system of atoms undergoing dynamical motions such as vibrations and rotations of atoms. A 1 fs time step was used in all the MD simulations. During equilibration runs, the LAMMPS software restricts the periodic boundary conditions to a rectilinear shape. The xyz dimensions can be coupled when a barostat is applied, which can be used to retain a cubic geometry. The simulation of the unreacted monomers was run with MD using a constant pressure-constant temperature (NPT) algorithm. The xyz box dimensions were coupled in order to maintain a cubic geometry. This was run for 2×10^5 time steps (200 ps). The final configuration was taken and used for the

construction of the crosslinked epoxy. Fig. 3 shows the atoms contained within the

constraints of a periodic boundary condition cell. The edge length of this cubic cell is

approximately 4 nm. The x and z coordinates lie in the plane of the figure.

The final configuration of atomic coordinates of the reactant mixture is used to

form a crosslinked network by the addition of chemical bonds consistent with the

chemical reactions depicted in Fig. 2. Epoxide groups react with amine groups to form

chemical bonds resulting in a complex network structure. In order to form the network,

the distances between atoms which will be connected by crosslinked chemical bonds

must be calculated. The first step is to calculate all the distances between all possible

pairs of the terminal carbon atoms in the epoxide functional groups and the nitrogen

atoms in the amine groups. The second step is to tabulate a list of potential bonds

between the epoxy terminal carbons and the amine nitrogens, prioritizing by shortest

distance. The bonding is restricted such that each epoxy terminal carbon is bonded to a

maximum of one amine nitrogen and that each amine nitrogen is bonded to a maximum

of two epoxy terminal carbons. The formation of these bonds will be restricted on the

basis of a cutoff radius, r_{cutoff}, between these atom pairs. An r_{cutoff} value greater than 7-8

Å will typically result in configurations which are difficult to equilibrate with

conventional MM and MD techniques. The final step is to form these bonds. The

hydrogen atom that is attached to the reacting nitrogen is then bonded to the epoxide

group, forming an alcohol as depicted in Fig. 2a. This new crosslinked structure is then

used for the MM/MD simulation.

The newly created atomistic configuration must be carefully equilibrated since the

use of a relatively large cutoff radius, r_{cutoff}, results in unrealistic bond lengths. A short

initial energy minimization is applied to the structure using a conjugate gradient algorithm in the LAMMPS software with an energy delta tolerance of 10^{-4} kcal/mol. This is followed by an NPT MD simulation at a temperature of 300 K and a pressure of 1 atm for 2×10^5 time steps (200 ps). The procedure described in the above paragraph can be repeated in order to increase the degree of crosslinking, α. The degree of crosslinking, α, is a unitless fraction with a maximum value of 1.0 for this stoichiometrically equivalent system. When α is equal to 1.0, all epoxide groups are bonded to an amine and each amine is bonded to 2 epoxide groups. By specifying r_{cutoff} and by choosing the number of iterations of the procedure, models with a range of α values can be obtained.

Once the desired degree of crosslinking, α, is achieved, a more complete equilibration is applied. An energy minimization procedure is applied with a restriction of energy delta tolerance of 10^{-4} kcal/mol. The structure was simulated with MD for 10^5 time steps (10^2 ps) at 450 K using an NPT algorithm with no coupling between the three box dimensions. The dimensions remain nearly cubic however. Subsequently, the temperature was reduced linearly by 25 K over a simulation period of 20 ps. This was followed by 100 ps of MD simulation at 425 K. This procedure is repeated in stepwise manner down to 300 K. The final trajectory at each temperature is saved for running deformation simulations.

In order to create atomistic models with moisture present, water molecules were added randomly to the structures. Water molecules were added at 5 and 9.5 wt. %. Following the addition of water molecules, energy minimization was applied. The structures were then subsequently equilibrated with MD from 450 K to 300 K using the stepwise cooling procedure described in the previous paragraph.

In order to obtain additional configurations for running deformation simulations, the MD simulation was run for an additional 100 ps. The final trajectory at each temperature is saved for running deformation simulations. The MD simulation was repeated for another 100 ps in order to obtain 3 separate atomistic configurations with their associated velocities for a given degree of crosslinking (α), moisture content (f_{water}), and temperature (T). Although 10^5 time steps (10^2 ps) does not result in drastically distinct configurations, the properties calculated from these configurations did show statistical variation.

One major statistical variation that was not included is the building of independent structures through the crosslinking reaction process. Since the reactant molecules were randomly mixed, the crosslinked structures could be built with different molecular configurations, despite having the same value of α. For the current work, however, with consideration of the computational resources required to run the MD simulations, multiple independent structures with identical parameter values were not built.

2.2. Method for calculating elastic constants

The method used here for calculating the elastic constants is similar to a method for static deformation of periodic atomistic models[13], but applied to a dynamic simulation in a constant volume-constant temperature (NVT) ensemble. The 6x6 elastic constant matrix **C** is determined by the partial derivatives of the stress tensor, τ, with respect to the deformation, ε, as indicated by Eq. 1.

$$C_{LMNK} = \left. \frac{\partial \tau_{LM}}{\partial \varepsilon_{NK}} \right|_{T,\varepsilon(NK)} \tag{1}$$

A series of deformations are applied to the periodic boundary cell in order to estimate values of these partial derivatives. These deformations are the following: A uniaxial deformation is applied to the x coordinate. The remaining two dimensions (yz) are unchanged. This is repeated for the y and z coordinates while keeping the remaining (xz and xy, respectively) coordinates fixed. Likewise, three shear deformations are applied. All deformations are in the positive direction, such that the periodic boundary coordinate x is increased during a uniaxial deformation along x for instance. These deformations are performed in an NVT ensemble using the LAMMPS simulation software. The deformation is applied in a continuous fashion at every time step at a constant rate with respect to the original dimensions. For most of the deformations, the periodic boundary cell was deformed by 5% over a simulation period of 10^2 ps (10^5 time steps). This is a relative deformation rate of 5×10^8 s^{-1} or 0.02 Å/ps. Though high by experimental standards, these are typical rates of deformations for MD simulations[23, 24]. The stress tensor was recorded at 10 time step (10 fs) intervals leading to a collection of 10^4 data points. This stress is calculated from the virial stress formula. These are usually averaged in batches of 10^3 time step intervals (10 ps). For example, in the case of the deformation of the x coordinate, the xx component of the stress tensor, τ_{xx}, is plotted as a function of the relative deformation, ε_{xx}, and the slope of this line is obtained. This value is placed in the first column, first row in the $\mathbf{C}$ elastic constant matrix. From the same simulation, plots of τ_{yy} and τ_{zz} versus the degree of deformation, ε_{xx}, are obtained. These are placed in the 2nd and 3rd row of the 1st column of the $\mathbf{C}$ elastic matrix. The first three columns of the $\mathbf{C}$ matrix are therefore obtained from the three tension simulations in x, y and z. The last three columns are obtained from the three shear deformation simulations.

Therefore, the entire 6x6 **C** matrix is generated. For this amorphous polymer model, isotropic symmetry is assumed. A least squares fitting method is used to obtain the elastic constants, μ and λ from Eqs. 2-6. [25]

$$\mu = \frac{4a - 2b + 3c}{33} \tag{2}$$

$$\lambda = \frac{2a + c - 15\mu}{6} \tag{3}$$

$$a = C_{11} + C_{22} + C_{33} \tag{4}$$

$$b = C_{12} + C_{13} + C_{21} + C_{23} + C_{31} + C_{32} \tag{5}$$

$$c = C_{44} + C_{55} + C_{66} \tag{6}$$

The Young's modulus, E, and shear modulus, G, can then calculated from Eqs. 7-8.

$$E = \mu \frac{3\lambda + 2\mu}{\lambda + \mu} \tag{7}$$

$$G = \mu \tag{8}$$

3. Results

In this section, the results obtained from the methods applied in section 2 are presented. Details associated with the construction of the atomistic epoxy models are noted. This is followed by the results obtained from the applied deformation of the equilibrated models.

3.1. Construction of the epoxy models

Four atomistic structures with different degrees of crosslinking, α, were built. The two highly crosslinked structures, ($\alpha = 0.86$, 0.80) required two successive

crosslinking reactions as described in section 2.1. The two with relatively low degree of crosslinking ($\alpha = 0.56$, 0.38) were obtained with only one crosslinking reaction. Fig. 4 shows an example result of the degree of crosslinking, α, obtained by using various cutoff radius values, r_{cutoff}. The filled squares indicate the value of α which would be obtained in the first crosslinking reaction as a function of r_{cutoff}. The open circles indicate the total value of α obtained as a function of r_{cutoff} after the first crosslinking was applied using a cutoff radius value of 8 Å. This indicates that it is possible to obtain highly crosslinked structures with only two cycles of the procedure.

The equilibration procedure described in section 2 was applied to all four epoxy models. Fig. 5 shows the density, ρ, calculated as a function of temperature, T, for one of these equilibration simulations ($\alpha = 0.80$, and $f_{water} = 0$ wt. %). The density and temperature are sampled every 1 ps during the 100 ps run. The last 50 ps of these data values are averaged while the first 50 ps are ignored in order to allow the model to come to equilibrium at each new temperature. The error bars shown in Fig. 5 are obtained from the standard deviations of these averages. Although such plots are often used to estimate the glass transition temperature, T_g, this is not attempted here. The results indicate the expected decrease in density with increasing temperature, with a final density at 300 K (1.08 g/cm^3) slightly lower than typically seen experimentally (1.16 g/cm^3) [26]. The final density for the highest degree of crosslinking ($\alpha = 0.86$, and $f_{water} = 0$ wt %) is only slightly greater (1.09 g/cm^3). Using the data from a restricted temperature range ($T = $ 300-375 K), the volumetric coefficients of thermal expansion (CTE) are calculated. The data are restricted in this way to avoid the glass transition temperature and the boiling point of water. Table 1 shows these values for the twelve structures that were simulated.

In the case of high degree of crosslinking and no moisture present ($\alpha = 0.86, f_{water} = 0$ wt. %), the CTE is 278 (x10^{-6}) K^{-1}. A recent experimental paper[17] lists a linear CTE of 79.99 (x10^{-6}) $^{\circ}$C^{-1} for a DGEBA-DETDA epoxy. This would correspond to a volumetric CTE of 240 (x10^{-6}) K^{-1} which is in the same general range as the value in row one of Table 1. Generally, the CTEs increase with increasing moisture content and decreasing degree of crosslinking, although there are some inconsistencies. The most notable inconsistencies are with the ($\alpha = 0.80$) values. The ($\alpha = 0.80, f_{water} = 0$ wt. %) value is lower than that for ($\alpha = 0.86, f_{water} = 0$). Also, the CTE value actually decreases from ($\alpha = 0.80, f_{water} = 5$ wt. %) to ($\alpha = 0.80, f_{water} = 9.5$ wt. %).

Following equilibration of each of the four neat equilibrated epoxy structures, water molecules were added at both 5 wt. % (135 water molecules) and 9.5 wt. % (270 water molecules). The equilibration procedure was repeated as described in section 2.2. A total of 12 distinct atomistic structures were created with the variation in α (= 0.86, 0.80, 0.56, 0.38) and f_{water} (= 0, 5, 9.5 wt. %). Instantaneous snapshots of the positions and velocities of the atoms of the structures were preserved at a range of temperatures from the equilibration simulation.   Snapshots were chosen from three temperatures ($T = 300$ K, 350 K, 400 K) as starting points to run deformation simulations.

3.2 Mechanical properties of the models

In this section, results are presented for the calculation of elastic constants of the models. We expect to see the moduli decrease for increasing temperature (T), reduced degree of crosslink (α) and increased water content (f_{water}). Generally, these trends are observed with some inconsistencies. As noted in section 1, the relationship between the aging process and these structural features (α, f_{water}) can be quite complex even under

controlled laboratory conditions. Therefore, we do not discuss the effects of aging directly, but rather consider the results of the calculations as a function of the controlled structural variables.

Fig. 6 shows a plot of the stress tensor component τ_{xx} as a function of the degree of strain deformation in the x direction, ε_{xx}. These values are averages over 1000 data points taken at 10 time step intervals. Therefore, each data point is averaged over a duration of 1 ps. These values over the 10 ps interval fall on a linear slope. The slope of this line is shown in Fig. 6, calculated from a least squares fit of the averaged values. The partial derivative ($\partial\tau_{xx}/\partial\varepsilon_{xx}$), is estimated as the slope of this line.

A large number of relatively short MD simulations were run in order to collect the data for the mechanical properties. With 4 values of α, 3 values of f_{water}, and 3 values of T, there are 36 variations in the parameter set. With the 3 sample configurations for each parameter set, there are 108 distinct configurations for running deformation simulations. Each of these has six deformation simulations applied to it, for a total of 648 MD deformation simulations. As detailed in section 2.2, the results from the 6 deformations are averaged using a least squares procedure to obtain the two Lamé constants, λ and μ, from which the elastic constants can be defined. The elastic constants from the three independent configurations with the same set of parameters (α, f_{water}, T) are then averaged and the standard deviation is calculated.

Fig. 7 shows the Young's modulus, E, as a function of crosslink degree, α, calculated from atomistic models with no moisture content ($f_{water} = 0$ wt. %). The three lines are shown for data calculated at three temperatures: 300 K, 350 K and 400 K. The values shown are taken from the average of the three configuration runs for a given set of

parameter values. The error bars shown are taken from the standard deviations of these three data values. Some error bars are actually smaller than the symbols and are therefore not readily visable. Generally, there is an increase in E with increasing α, within the limits of the error bars. At the two highest values of α, there seems to be a decrease in E. This slight decrease is most likely due to statistical error. The maximal values for the two highest crosslinking densities at 300 K are 2.8 ± 0.2 GPa and 2.6 ± 0.1 GPa. This compares well with recent experimental measurements of DGEBA-DETDA epoxy which was measured at 2.7GPa[27]. Fig. 8 shows the shear modulus, G, as a function of α for three different values of temperature. The trends follow those from Fig. 7, which is to be expected from the least squares fitting procedure described in section 2.2.

Fig. 9 shows the Young's modulus, E, as a function of the temperature, T, for three values of moisture content, $f_{water} = 0$, 5 and 9.5 weight %. The crosslink density, α, is fixed at 0.80. The modulus declines with increasing T for all values of f_{water}, however the trends are not completely as expected as the lines cross. Ideally, all values would decline consistently with increasing f_{water} and decreasing α. It appears that it is much more difficult to get reliable or expected trends as a function of moisture content as compared to as a function of temperature and crosslink degree. This may be due to the limitations of the modeling capability and current hardware/software technology. However, experimental findings have suggested a complex structure of water within the epoxy[1, 2, 28]. This will require further analysis, but is beyond the scope of this paper.

Fig. 10 shows the same plot as Fig. 9, but with $\alpha = 0.38$. Here, the Young's modulus decreases to very low values at 400 K, when moisture is present. For $\alpha = 0.80$ and no moisture, the modulus decreases by 35% with an increase in temperature from

300 K to 400 K, whereas the same change in conditions for $\alpha = 0.38$ results in a 70% decrease in modulus. Considering the plot, it would appear that the low value of α is most influential in lowering E at higher temperatures as compared to the moisture content.

Fig. 11 shows the Young's modulus, E, as a function of moisture content, f_{water}, for the epoxy simulations at 300 K. In most cases, a consistent decline in E with increasing water content is seen. The data for $\alpha = 0.86$ are less consistent, however, which illustrates that these simulations are less reliable in calculating properties dependent on moisture content. Another important point is to note that the Young's modulus, E, is greater for $\alpha = 0.80$ than for $\alpha = 0.86$ in all values of f_{water} except 9.5 wt. %. This value at $\alpha = 0.86$ and $f_{water} = 9.5$ wt. % is the only case in this graph where E does not decrease consistently with increasing f_{water}. Fig. 12 shows the Young's modulus, E, as a function of moisture content, f_{water}, for the epoxy simulations at 350 K. In this case, the results appear to exhibit the expected dependencies (decline in E with decreasing α and increasing f_{water}) more closely than in Fig. 11. Among the results that are not expected are the following: At $f_{water} = 0$ wt. %, E is slightly lower for $\alpha = 0.80$ than for $\alpha = 0.86$. For $\alpha = 0.80$, E increases slightly as f_{water} increases from 5 to 9.5 wt. %, although, this increase is below the standard deviation calculated for either value. For $\alpha = 0.38$, E increases slightly as f_{water} increases from 0 to 5 wt. %, although, this increase is below the standard deviation calculated for either value.

Fig. 13 shows the Young's modulus, E, as a function of moisture content, f_{water}, for the epoxy simulations at 350 K. A notable aberration is the slight increase in E as f_{water} increases from 0 to 5 wt. %, with $\alpha = 0.86$. This increase is below the standard deviation calculated for E with $f_{water} = 5$ wt. % and $\alpha = 0.86$.

4. Conclusions

The motivation of this work was to study the difficult to predict effects of hygrothermal aging on epoxies. Because of the complicated nature of the relationship between these structural parameters (α, f_{water}) and the aging process even under controlled laboratory conditions, the aging effects are studied indirectly. Atomistically detailed models of crosslinked epoxies were constructed with a range of degree of crosslinking (α) and moisture content (f_{water}). The elastic constants were calculated for these models. The moduli were found to decrease consistently with increasing temperature. There was a relatively consistent dependency of the moduli on the degree of crosslinking, α, with these moduli values decreasing with decreasing α. A less consistent dependency was found on the moduli as a function of moisture content.

For each model with a specific value of parameters (α, f_{water}, T), there were 3 different samples. These samples were obtained as different configuration snapshots from a MD trajectory separated by 1×10^5 time steps (100 ps). Although this is a relatively short time span, the values obtained from these different configurations had statistical variation as indicated by the error bars in Figs. 7-13. Some additional averaging is obtained by the assumption of isotropic behavior and the fitting indicated by Eqs. 2-6.

Although statistically independent configurations with identical parameter sets were not constructed, variation was addressed by the use of configurations generated from MD simulation trajectories. In addition, by assuming isotropic symmetry and averaging over deformations applied to the various coordinates, an additional structural averaging was achieved.

Acknowledments

α	f_{water} (wt. %)	Volumetric CTE (K^{-1})
0.86	0	278.
	5	286.
	9.5	360.
0.80	0	188.
	5	391.
	9.5	375.
0.56	0	360.
	5	425.
	9.5	477.
0.38	0	405.
	5	500.
	9.5	584.

Table 1. The volumetric coefficients of thermal, CTE, expansion.
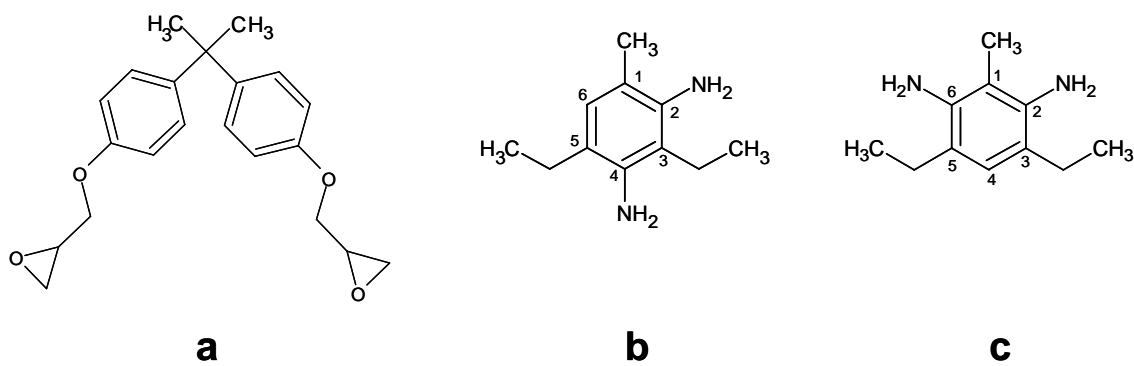
Fig. 1. a) Diglycidyl ether of bisphenol A (DGEBA). b) 3,5-Diethyltoluene-2,4-diamine. c) 3,5-Diethyltoluene-2,6-diamine. (DETDA)

a

R —NH$_2$ + CH$_2$—CH— (epoxide, O bridge) ⟶ R —NH —CH$_2$—CH— (OH)

b

R —NH —CH$_2$—CH— (OH) + CH$_2$—CH— (epoxide, O bridge) ⟶ R —N —CH$_2$—CH— (OH), with HC—OH / CH$_2$ substituent
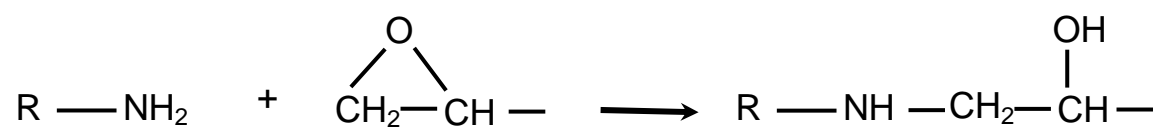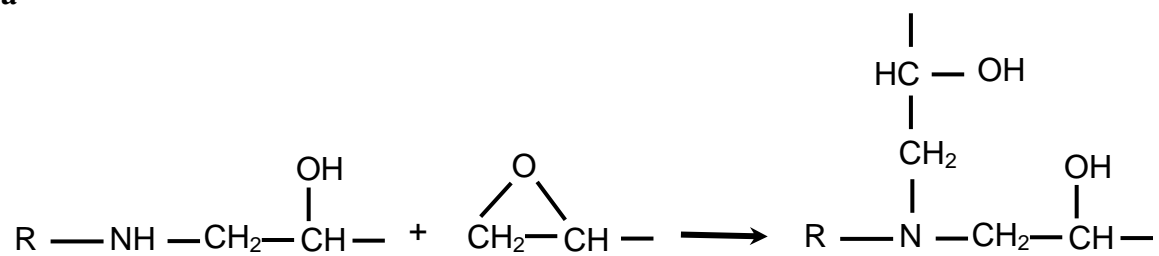
Fig. 2. The chemical reaction of an epoxide with an amine.
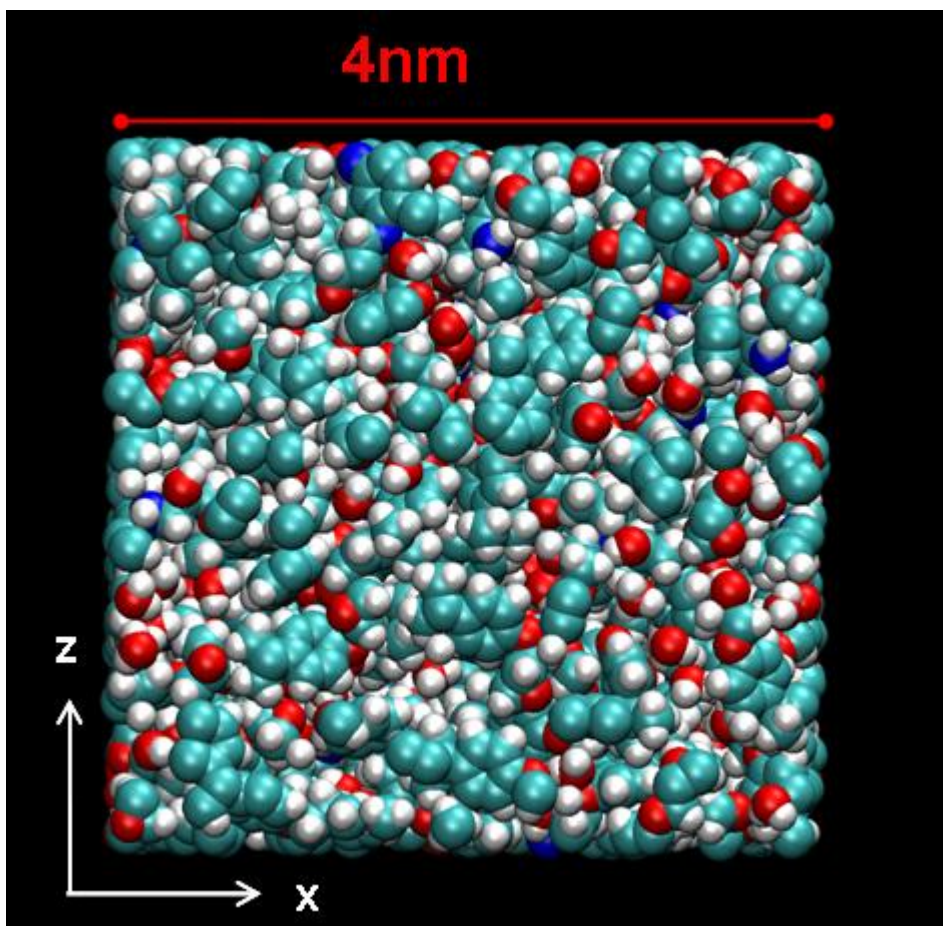
Fig. 3. The atoms of the epoxy simulation contained with the constraints of the periodic boundary conditions. The cartesian coordinate reference system is shown with respect to the structure.
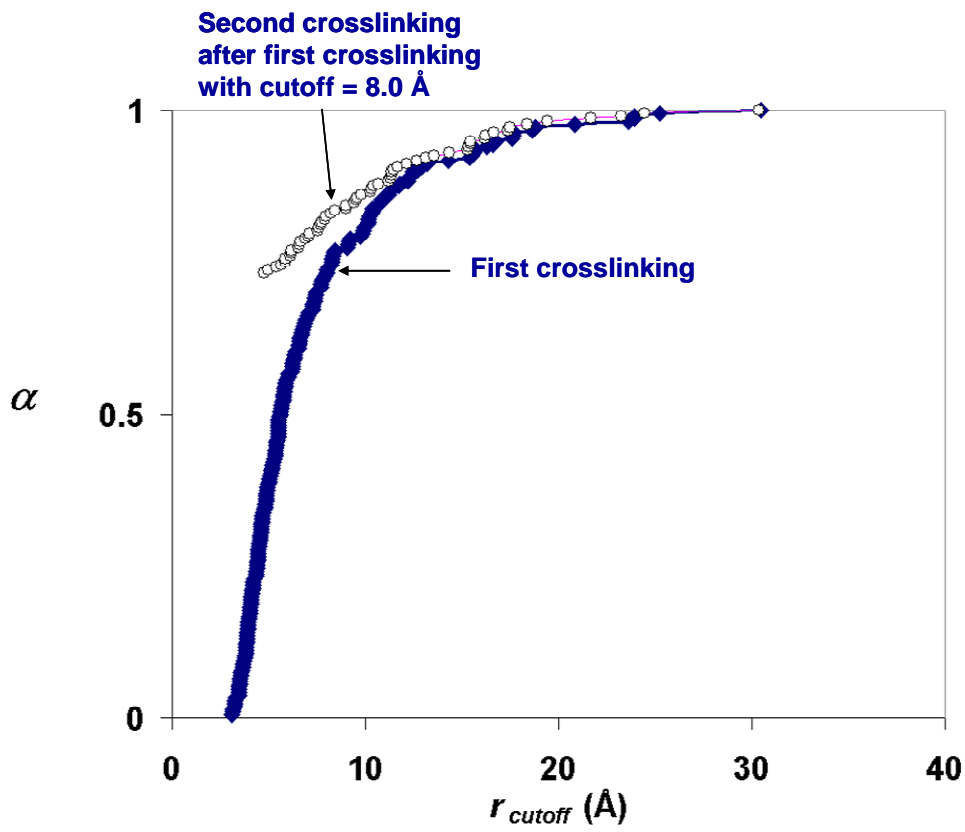
Fig. 4. Degree of crosslinking, α, as a function of cutoff radius r_{cutoff}.
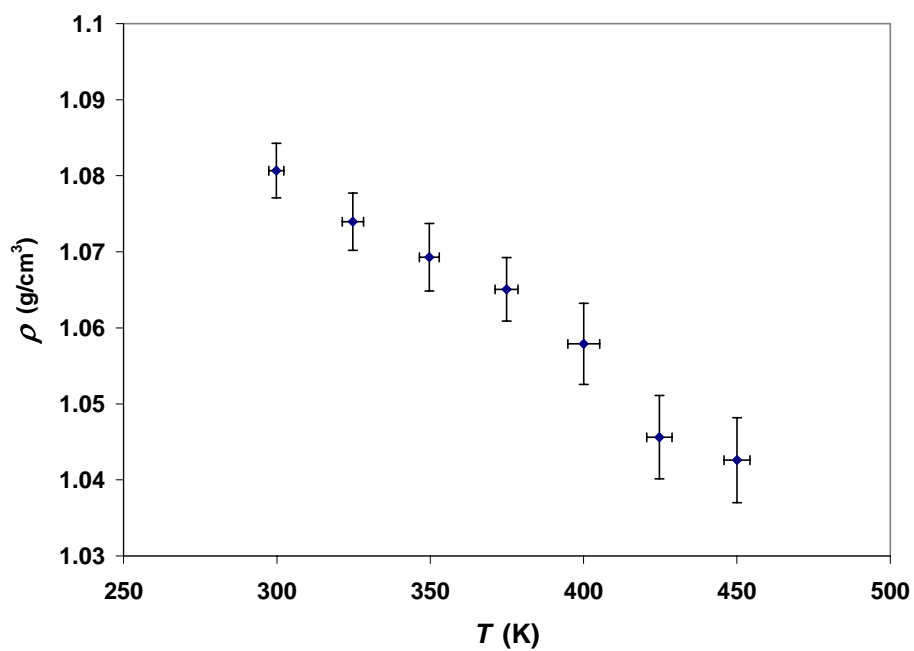
Fig. 5. The density, ρ, is plotted as a function of temperature, T, for a sample with $\alpha =$ 0.80, and $f_{water} = 0$ wt. %.
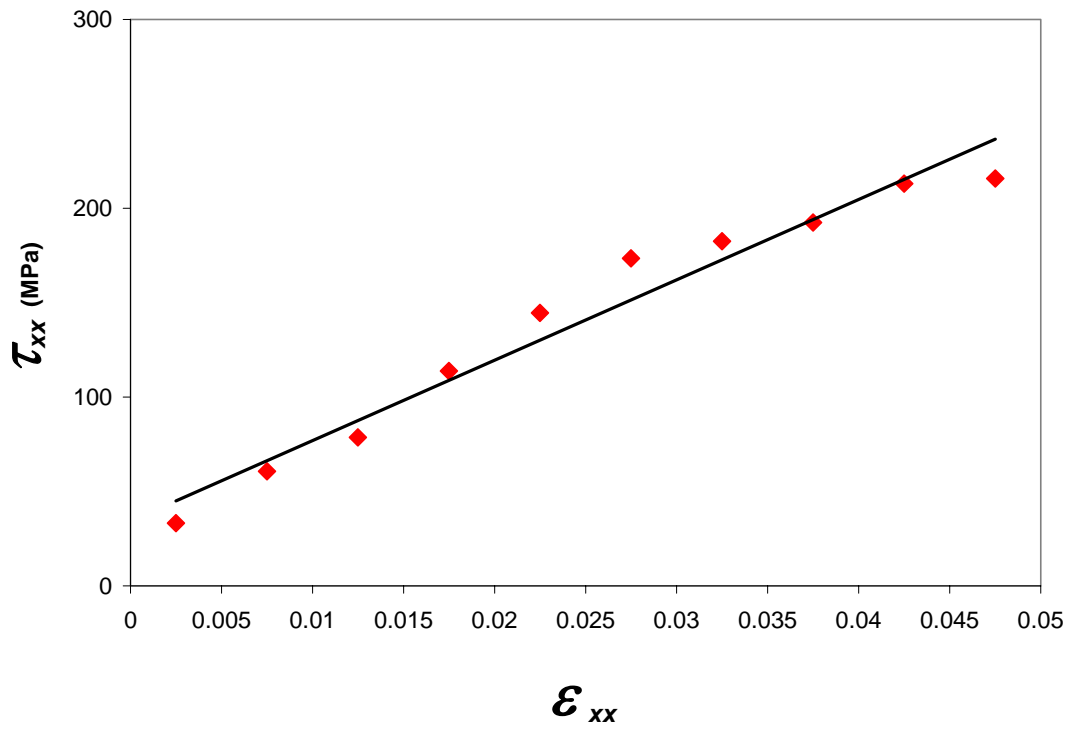
Fig. 6. The *xx* component of the stress tensor, τ_{xx}, as a function of the strain in the *x* direction, ε_{xx}. These data is taken from the $\alpha = 0.80$, $f_{water} = 0$ wt. % system.
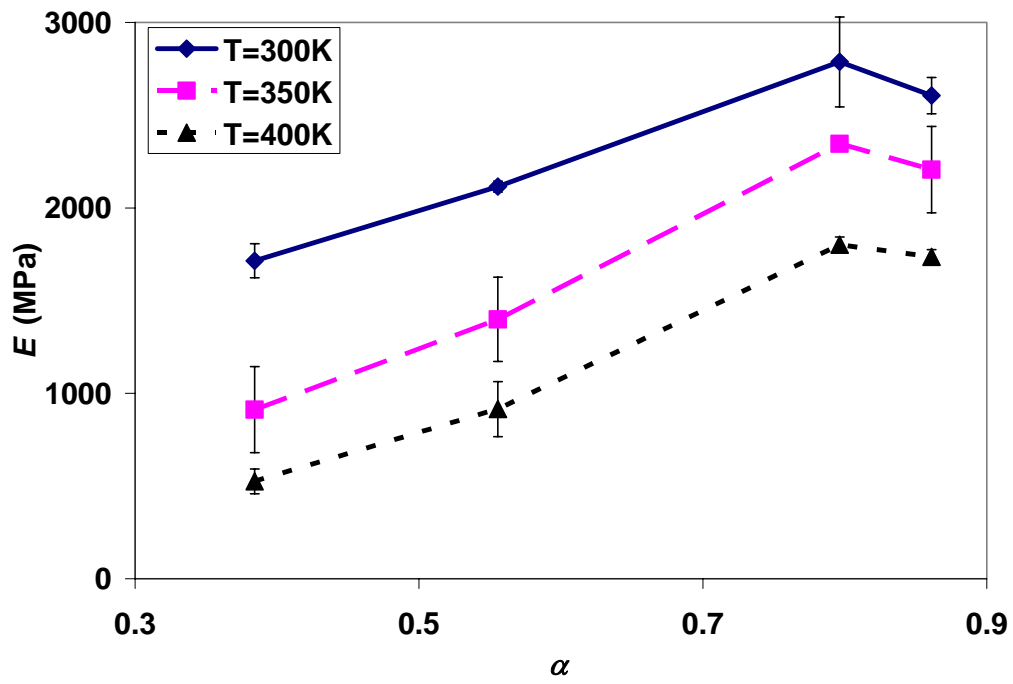
Fig. 7. The Young's modulus, E, as a function of crosslink degree, α, for three different temperatures. These values are shown for samples with no moisture content ($f_{water} = 0$ wt. %).
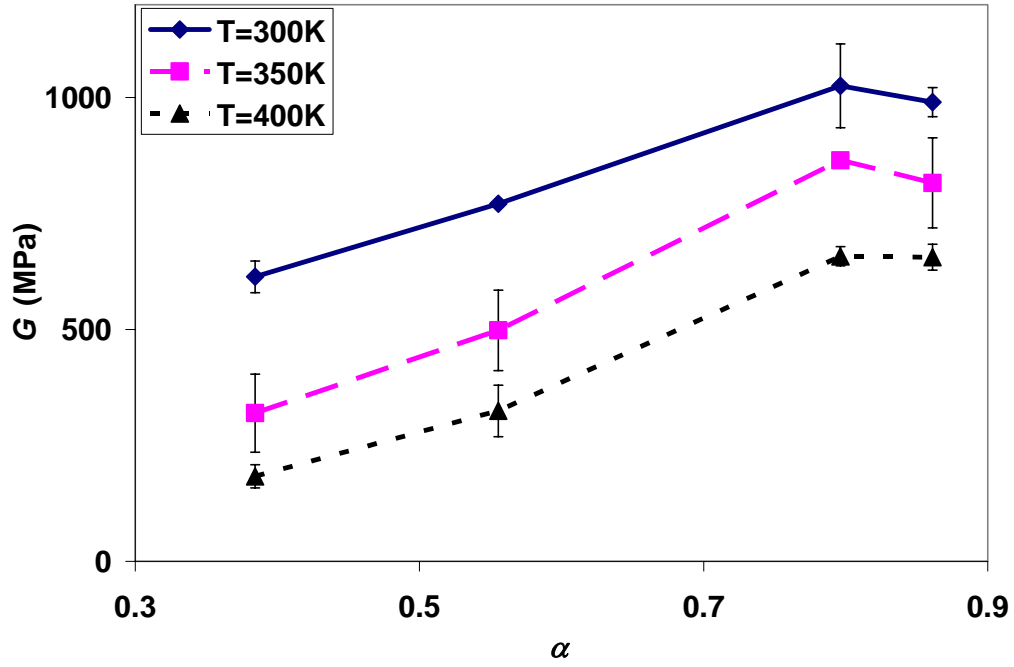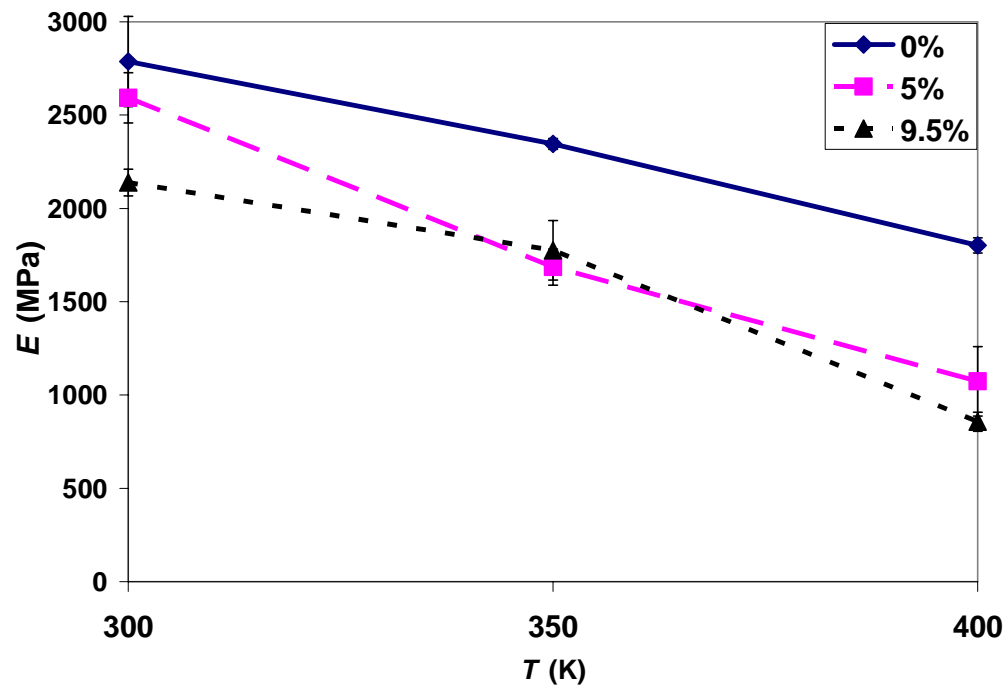
Fig. 8. The shear modulus, G, as a function of crosslink degree, α, for three different temperatures. These values are shown for samples with no moisture content ($f_{water} = 0$ wt. %).

Fig. 9. The Young's modulus, E, is plotted as a function of temperature, T, for three values of the moisture content ($f_{water} = 0$, 5, 9.5 wt. %) and with degree of crosslinking, $\alpha = 0.80$.
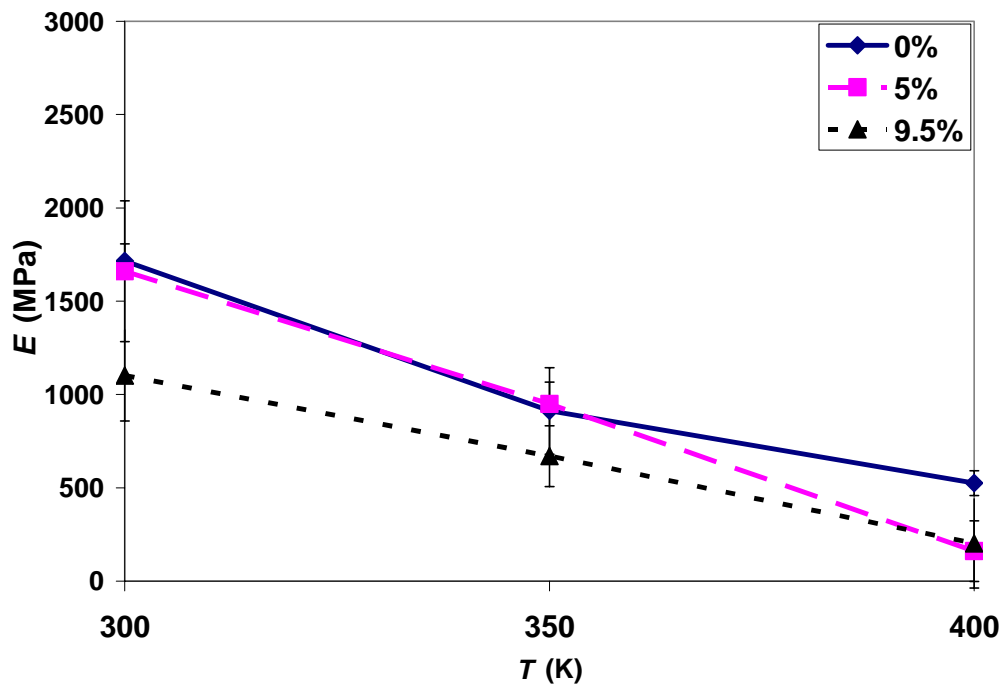
Fig. 10. The Young's modulus, E, is plotted as a function of temperature, T, for three values of the moisture content ($f_{water} = 0$, 5, 9.5 wt. %) and with degree of crosslinking, $\alpha = 0.38$.
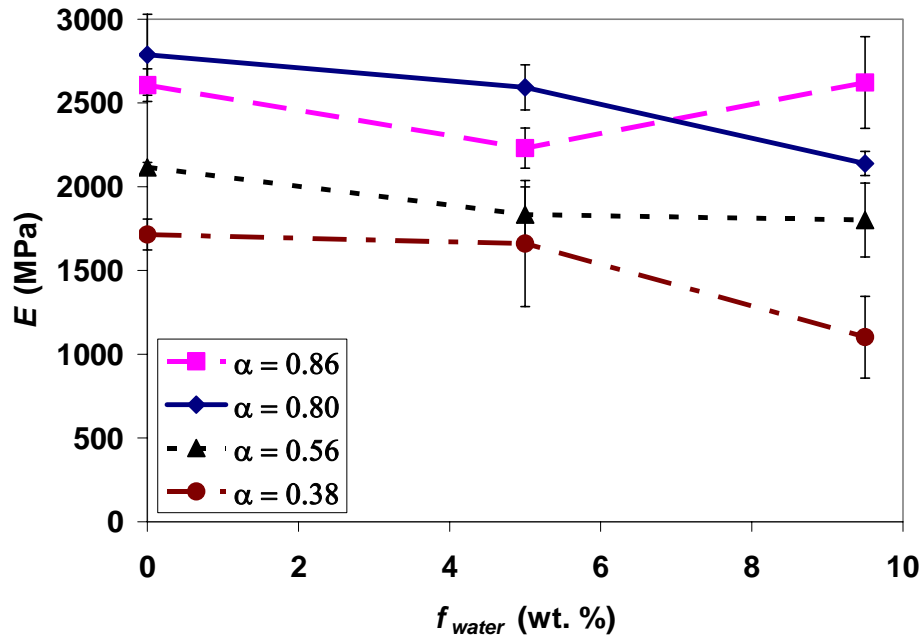
Fig. 11. The Young's modulus, E, as a function of moisture content, f_{water}, at 300 K.
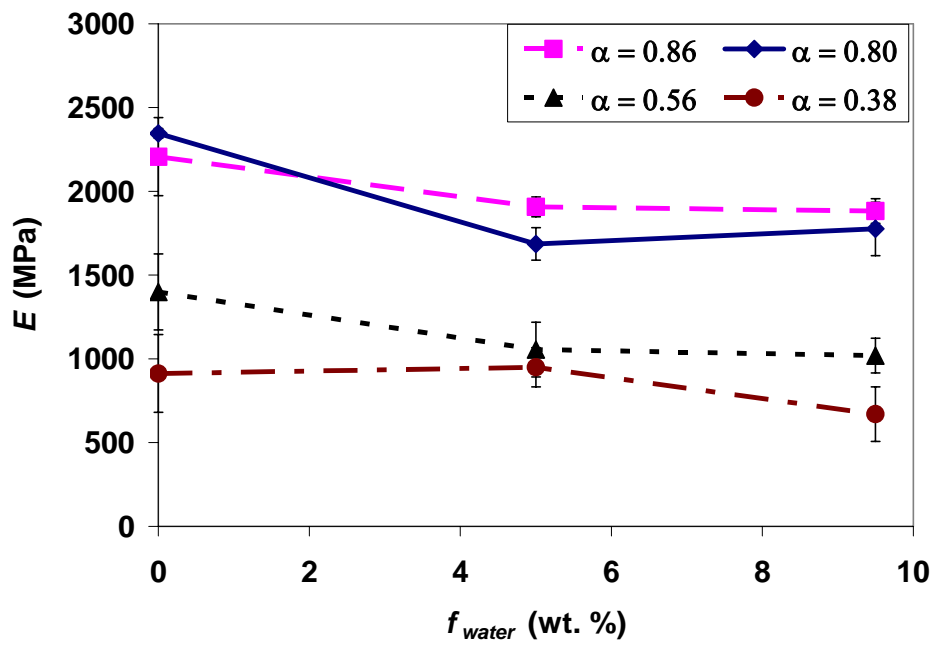
Fig. 12. The Young's modulus, E, as a function of moisture content, f_{water}, at 350 K.
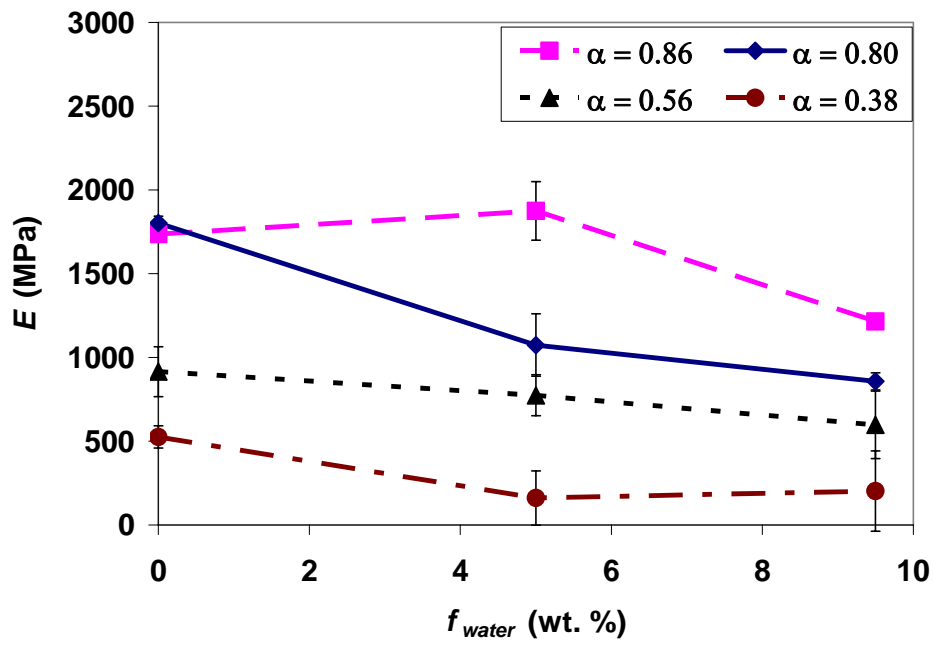
Fig. 13. The Young's modulus, E, as a function of moisture content, f_{water}, at 400 K.

References

[1]   Popineau S, Rondeau-Mouro C, Sulpice-Gaillet C, Shanahan MER. Polymer 2005;46:10733-10740.
[2]   Zhou JM, Lucas JP. Polymer 1999;40:5505-5512.
[3]   Chatterjee A, Gillespie JW. J. Appl. Polym. Sci. 2008;108:3942-3951.
[4]   Zhou JM, Lucas JP. Polymer 1999;40:5513-5522.
[5]   Moy P, Karasz FE. Polym. Eng. Sci. 1980;20:315-319.
[6]   Peyser P, Bascom WD. J. Mater. Sci. 1981;16:75-83.
[7]   Xiao GZ, Delamar M, Shanahan MER. J. Appl. Polym. Sci. 1997;65:449-458.
[8]   Yang QA, Xian GJ, Karbhari VM. J. Appl. Polym. Sci. 2008;107:2607-2617.
[9]   Yarovsky I, Evans E. Polymer 2002;43:963-969.
[10]   Varshney V, Patnaik SS, Roy AK, Farmer BL. 49th AIAA/ASME/ASCE/AHS/ASC Structures, Structural Dynamics and Materials Conference, Schaumburg, IL, April 7-10, 2008.
[11]   Wu CF, Xu WJ. Polymer 2006;47:6004-6009.
[12]   Varshney V, Patnaik SS, Roy AK, Farmer BL. Macromolecules 2008;41:6837-6842.
[13]   Theodorou DN, Suter UW. Macromolecules 1986;19:139-154.
[14]   Brown D, Clarke JHR. Macromolecules 1991;24:2075-2082.
[15]   Valavala PK, Clancy TC, Odegard GM, Gates TS. Int. J. Solids Struct. 2007;44:1161-1179.
[16]   Barton JM, Deazle AS, Hamerton I, Howlin BJ, Jones JR. Polymer 1997;38:4305-4310.
[17]   Liu WC, Varley RJ, Simon GP. Polymer 2006;47:2091-2098.
[18]   Wang JM, Cieplak P, Kollman PA. Journal of Computational Chemistry 2000;21:1049-1074.
[19]   Weiner PK, and Kollman, P. A. Journal of Computational Chemistry 1981;2:287-303.
[20]   Jorgensen WL, Chandrasekhar J, Madura JD, Impey RW, Klein ML. J. Chem. Phys. 1983;79:926-935.
[21]   Materials Studio$^{®}$ is a product of Accelrys, Inc., San Diego, CA, USA.
[22]   Plimpton S. Journal of Computational Physics 1995;117:1-19.
[23]   Capaldi FM, Boyce MC, Rutledge GC. Polymer 2004;45:1391-1399.
[24]   Lyulin AV, Balabaev NK, Mazo MA, Michels MAJ. Macromolecules 2004;37:8785-8793.
[25]   Suter UW, Eichinger BE. Polymer 2002;43:575-582.
[26]   Ratna D, Varley R, Raman RKS, Simon GP. J. Mater. Sci. 2003;38:147-154.
[27]   Qi B, Zhang QX, Bannister M, Mai YW. Compos. Struct. 2006;75:514-519.
[28]   Chatteriee A, Gillespie JW. J. Appl. Polym. Sci. 2008;108:3942-3951.